Strain induced electrochemical behaviours of ionic liquid electrolytes in an Electrochemical Double Layer Capacitor: Insights from molecular dynamics simulations

Tribeni Roy[1,2,3*], Saurav Goel[3,4] , Luciano T. Costa[5], Maria-Magdalena Titirici[6], Gregory J. Offer[1], Monica Marinescu[1], Huizhi Wang[1, *]

[1]Department of Mechanical Engineering, Imperial College London, SW7 2AZ, UK
[2]Department of Mechanical Engineering, Birla Institute of Technology and Science Pilani, Pilani Campus, 333031, India
[3]London South Bank University, 103 Borough Road, London SE1 0AA, UK
[4]Department of Mechanical Engineering, University of Petroleum and Energy Studies, Dehradun, 248007, India
[5]MolMod-CS, Institute of Chemistry, Universidade Federal Fluminense, CEP 24020-141, Niteroi-RJ, Brazil
[6]Department of Chemical Engineering, Imperial College London, SW7 2AZ, UK
Corresponding authors: *tribeni.roy@pilani.bits-pilani.ac.in*, *huizhi.wang@imperial.ac.uk*

Abstract

Electrochemical Double Layer Capacitors (EDLCs) with ionic liquid electrolytes outperform conventional ones using aqueous and organic electrolytes in energy density and safety. However, understanding the electrochemical behaviours of ionic liquid electrolytes under compressive/tensile strain is essential for the design of flexible EDLCs as well as normal EDLCs, which are subject to external forces during assembly. Despite many experimental studies, the compression/stretching effects on the performance of ionic liquid EDLCs remain inconclusive and controversial. Also, there is hardly any evidence of prior theoretical work done in this area, which makes the literature on this topic scarce. Herein, for the first time, we developed an atomistic model to study the processes underlying the electrochemical behaviours of ionic liquids in an EDLC under strain. Constant potential non-equilibrium molecular dynamics (MD) simulations are conducted for EMIM BF_4 placed between two graphene walls as electrodes. Compared to zero strain, low compression of the EDLC resulted in compromised performance as the electrode charge density dropped by 29%, and the performance reduction deteriorated significantly with a further increase of compression. In contrast, stretching is found to enhance the performance by increasing the charge storage in the electrodes by 7%. The performance changes with compression and stretching are due to changes in the double-layer

ESI available

structure. Also, an increase in the value of the applied potential during the application of strain leads to capacity retention with compression revealed by the newly performed simulations.

Keywords: Tension-compression asymmetry; Electrochemical Double Layer Capacitors; charge density; molecular dynamics; ionic liquids

1. Introduction

Global warming is an immediate concern. The current levels of CO_2 being released into the atmosphere need to decrease by 45% by 2030 and reach zero by 2050, according to the European green deal[1]. Consequently, there is a strong desire and massive ongoing efforts to revamp the transport sector by shifting to electric vehicles[2,3]. Recent developments in electric vehicles are aimed towards hybridising Li-ion batteries with Electrochemical Double Layer Capacitors (EDLCs) or Supercapacitors in order to overcome the limitations of long charging time and low-to-moderate power densities of Li-ion batteries[4,5]. The role of EDLCs is to contribute towards faster charging and prolonging the life of hybrid packs by taking a major share of power fluctuations of the vehicle. However, the application of EDLCs faces a challenge as they have a low energy density. The energy density of an EDLC is proportional to the capacitance and the square of the cell voltage, and the capacitance is proportional to the electrode surface area. Therefore, increasing the electrode surface area for enhanced capacitance or the cell voltage or a combination of the two will lead to increased energy density. Graphene as an electrode material has emerged as one of the potential candidates for increasing surface area and offers distinct advantages over activated carbons in terms of electrical conductivity, electrolyte adsorption, and mechanical stiffness[6,7]. On the other hand, ionic liquids offer a viable electrolyte considering their high electrochemical window of 4~5 V[8,9], compared to ~1.2 V for aqueous and ~2.7 V for organic electrolytes. Ionic liquids are also less volatile and have a high boiling point, so they can be safer and operate in a wider temperature range.

EDLC performance under strain has attracted much research interest due to the external pressure applied during EDLC assembly as well as the development of flexible EDLCs. Hyojin et al.[10] have developed a nature-inspired flexible carbon-based micro supercapacitor with an areal capacitance of 11.8 mF cm^{-2}, to power an implantable sensor. During compression, the

volumetric capacitance can increase due to the reduction of pore volume in the electrode. Since mass remains unchanged with mechanical loads, gravimetric capacitance provides a more sensible metric for studying compression effects. Li et al.[11] reported that the specific capacitance of EDLCs using single-walled carbon nanotube (SWNT) film electrodes increases with external loading, however, the trend for increase is different for different electrolytes and is dependent on ion size. Hu et al.[12] developed a flexible EDLC and found that compressing the cell by 60%, the electrochemical performance remain unaffected. Gourdin et al.[13,14] reported that compressing EDLCs with porous activated carbon electrodes would slightly increase capacitance during the initial loading, but have substantial impact on the porous structure of electrodes during the subsequent loading and possibly decrease the capacitance at higher compressive loads. A comparative analysis of compressive composite electrodes by Lv et al.[15] showed that compression of EDLCs using superelastic graphene aerogel can decrease the gravimetric capacitance of a cell. Similar results were also observed experimentally by Li et al.[16], who used carbon nanotube sponges as the electrode material. On the other hand, application of tensile strain or stretching of an EDLC was found to result in high capacity retention with strains of 200% and above[17,18]. Qianqian et al.[19] have developed a flexible supercapacitor based on self-stretchable polymer and carbon nanotubes, the device exhibited stable specific gravimetric capacity of 175.1 F/g under different flexibility tests. Nana et al.[20] developed an all-solid-state supercapacitor with a specific energy of 2.3 $mWhcm^{-3}$ based on polypyrrole nanofilms. Yongmin et al.[21] developed a metallic cellulose paper-based flexible supercapacitor with a power density of 15.1 $mW\ cm^{-2}$. Qing et al.[22] developed polydopamine crosslinked multifunctional hydrogel based flexible supercapacitor with a areal specific capacitance of 210.2 $mF\ cm^{-2}$ to power a pressure sensor.

Despite many studies, it is still debatable how compressive/tensile strain affects EDLC behaviours. The underlying fundamental principles are unclear, especially for ionic liquids

based EDLCs. The absence of solvent in ionic liquids is a major difference as compared to conventional aqueous and organic electrolytes. This leads to a different mechanism of double layer formation for ionic liquids. In the case of the conventional electrolytes, the presence of solvent in the electrolyte creates solvation around the ions and the double layer formed in such cases can be described using the classical Gouy-Chapman-Stern model for dilute electrolytes[23]. For ionic liquids which contain a high concentration of bare ions, the double layer formation cannot be explicitly explained by those conventional theories due to overscreening and crowding of ions near the electrode at increasing voltages[24]. To the best of the authors' knowledge, this is the first study elucidating the nanoscale insights on the performance of an ionic liquid based EDLC under externally applied stresses using constant potential non-equilibrium molecular dynamics (MD) simulations. The simulation made use of 1-ethyl-3-methylimidazolium tetrafluoroborate (EMIM BF_4) electrolyte as it is a commonly used ionic liquid electrolyte in EDLCs[25]. Various cases of compressive/tensile strains are studied, and their effects on electrode charge storage due to the double layer formation and retention of electrode charges as a result of compression and stretching are discussed.

2. MD simulation methodology

2.1. MD simulation model construction and boundary conditions

The EDLC was modelled as a simulation box of size 3.32 nm × 3.32 nm with a height of 6.74 nm (*z*-direction) including a 0.2 nm spacing on both side of the electrodes. The model contained 256 ion pairs of each type of ion ($EMIM^+$ and BF^-_4) placed between two parallel graphene electrodes (*Fig. 1*). Packmol software was used to build the initial geometry[26] while MD simulations were performed using LAMMPS software[27]. OVITO[28] was used for data analysis and visualisation. The length of the ionic liquid in the *z*-direction was maintained in such a way that the central region forms bulk phase and matches the experimental density of 1.294 g/mL at 25°C under no stress conditions. These dimensions were highly optimised from the initial bulk simulation carried out as 'a priori' to the main simulations. The initial simulations for preparing a box of ionic liquid (without electrodes) were performed by using the NVT ensemble where *x* & *y* axes were kept periodic while the walls of ionic liquid in the *z*-axis were made repulsive to reflect any atoms on approaching the *z* boundary of the box. Keeping the *z*-axis periodic during initial simulations render the bond lengths very high and hence electrode addition after this step can cause errors in simulation. An OPLS-AA force field was used to describe the ionic liquid[29] and electrode consisting of carbon atoms was described by the

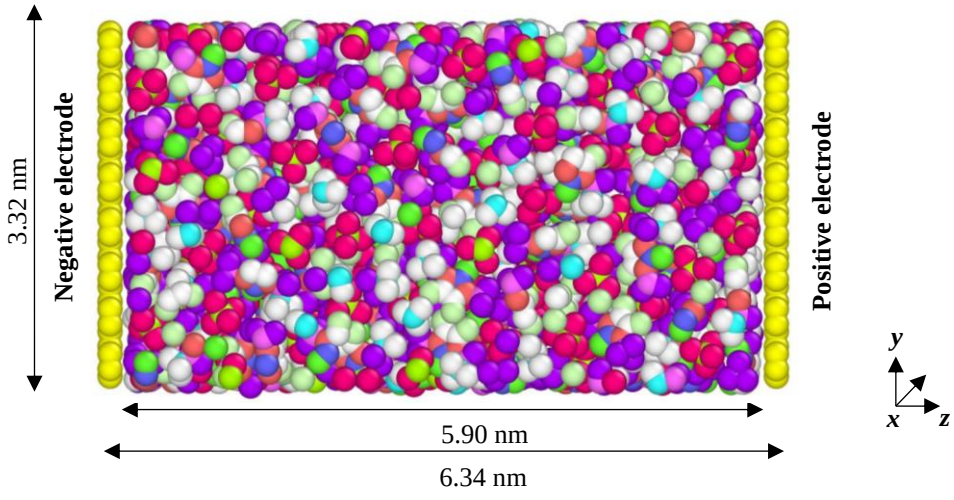

Fig. 1: MD model geometry showing the ionic liquid ($EMIM^+$ BF^-_4) placed between two graphene walls as electrodes

Lennard-Jones potential with a diameter of $\sigma_{LJ} = 3.4$ Å and potential well depth of $\varepsilon_{LJ} = 0.086$ kcal/mol. The Lorentz–Berthelot combination rule was used to simulate the interaction between different atomic species. The velocity Verlet algorithm was used for integrating the motion of particles with a timestep of 1 fs. The cut-off distance was kept as 14 Å for short-ranged potentials during all simulations and calculation of electrostatic interactions was carried out by using the particle−particle particle−mesh method (pppm) which is faster than the Ewald method[30]. A constant potential method was employed wherein the charges on electrode atoms follow Gaussian distribution and the charge fluctuations maintain a fixed potential difference between the electrodes[31]. To reduce computational costs, a single graphene wall was used on each electrode to resemble a three-layer graphite (Gaussian function parameter for each electrode = 19.79 nm^{-1}) [32].

2.2. Equilibration of the model

Initial simulation runs were carried out for 15 ns at 25°C in the NVT ensemble by applying 0V potential difference between the two graphene electrodes. The temperature during simulations was controlled using Nosé–Hoover thermostat with a relaxation time of 100 fs. This was done to ensure that the system is well equilibrated before carrying out production runs at a constant potential of $\varphi = 4.0\ V$ (for most cases). This equilibrated structure has been referred to as zero stress state (uncompressed) system throughout this study.

2.3. Dynamic run and data extraction

Once the equilibration process completes, a strain was applied. In this approach, the box length in the *z*-direction changes as per the function $z(t) = z_0(1 \pm lrate \times dt)$ where $lrate$ is the applied engineering strain rate $= 0.001/fs$, dt is the time elapsed and z_0 is the *z*-co-ordinate of the electrode in the zero stress/uncompressed state. The timestep for strain tests were taken

as 0.5 fs. During strain induced compression, $lrate$ was positive for the negative electrode and negative for the positive electrode (for stretched state i.e. during tension, it was opposite). 5 outputs were dumped for strain induced compression each after 2000 timesteps, $dt = 0.5 \times 2000fs = 1000\ fs = 0.001\ ns$. This means the total engineering strain $\frac{z(t)-z_0}{z_0}$ at each 2000th timestep ($0.001\ ns$) will be $0.001/fs \times 0.001\ ns = 1$ i.e. strain after $0.001\ ns$ (2000 timesteps) = 1, strain after $0.002\ ns$ (4000 timesteps) = 2, etc. and so on. In this paper, the minimum strain applied to the EDLC (considering both electrodes) was 2 and the maximum strain applied was 10. For the case of tension or stretching of EDLC, only 1 output was dumped at 2000 timesteps with strain = 1 on each electrode. During compression, the electrodes underwent compressive stresses due to reactive forces from the electrolyte while during stretching, tensile stresses were present on the electrodes. *Fig. 2* shows an example of true stress (during compression) acting on the electrodes with respect to the simulation time. Note that the stresses used in this study are higher than in practical devices to realise the deformation within nanoseconds timescale due to the limits of computational power. Though this can lead to different quantitative values, however, this would not affect the trend and thus the key

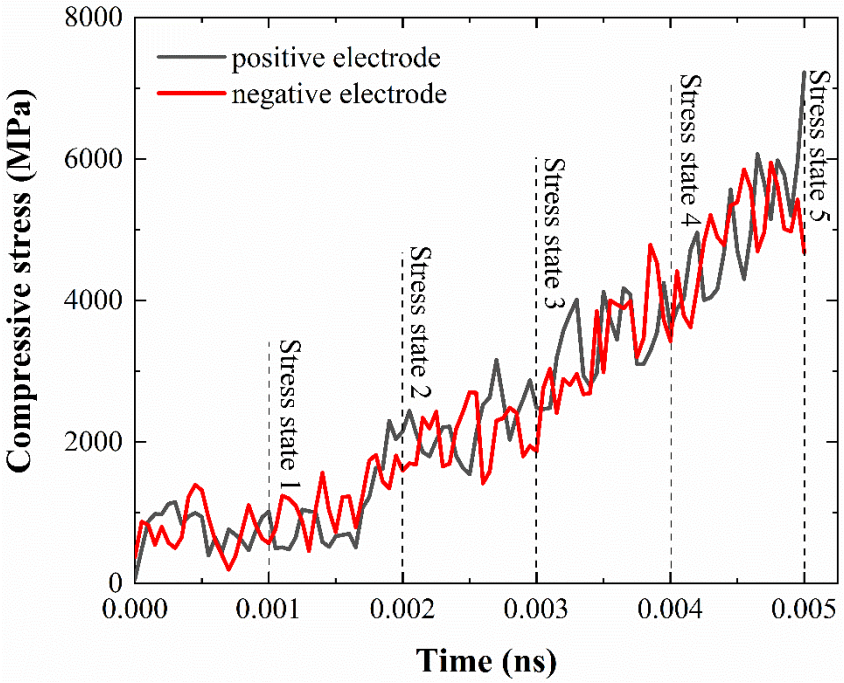

Fig. 2: Compressive stress on electrodes with time (absolute values shown)

conclusions of this study. *Supplementary Video 1* shows demonstration examples of an EDLC under different stress states. Stress state 1 indicates output of compressive strain at 2000th timestep, stress state 2 indicates output at 4000th timestep and so on. Stretching of the EDLC at zero stress state was carried out for one case by adopting a procedure similar to stress state 1 but by applying a tensile strain (*Supplementary Video 2*).

3. Results and discussion

3.1. Charging dynamics under compression

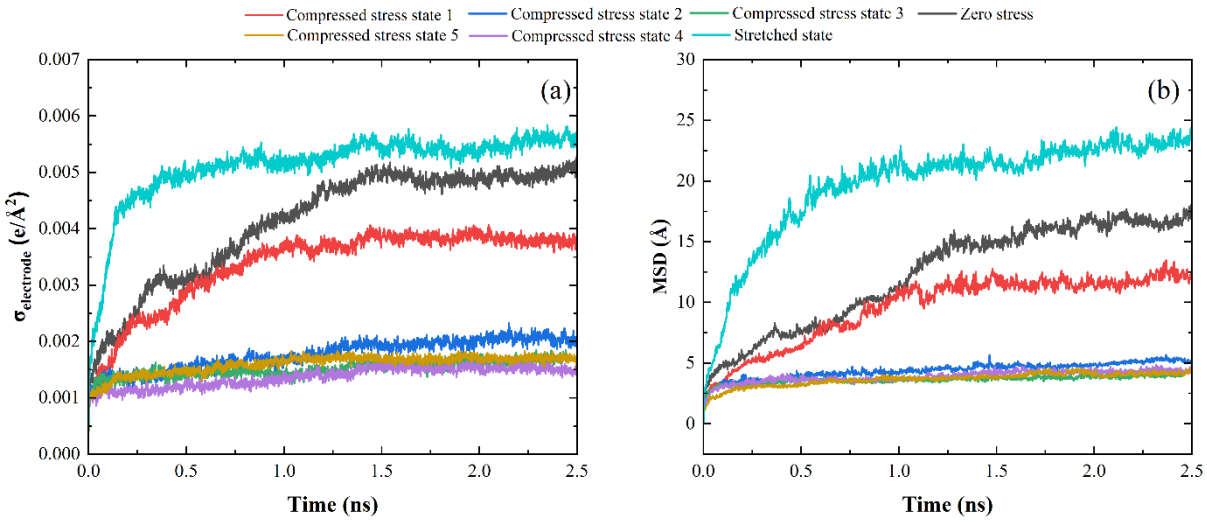

Fig. 3: (a) Electrode charge fluctuations and (b) mean square displacements under compression.

MD simulations were carried out at 4.0 V for different stress states as described in *Fig. 2*. The total time for simulations were limited to 2.5 ns since after this, no substantial charge fluctuations were observed thereby indicating that charging process is completed. The electrode charge fluctuations were calculated based on variation of electrode charge density with time.

$$\sigma_{electrode} = \frac{q_{electrode}}{A}. \qquad \ldots (1)$$

where $\sigma_{electrode}$ is the charge density on the electrode ($e/Å^2$), $q_{electrode}$ is the total charge on the electrode (e) and A denotes electrode surface area ($Å^2$). As the variations of electrode charge

density are similar for both the electrodes of a symmetric EDLC as shown in *Fig. S1*, for simplicity, all results presented in this study are shown with respect to the positive electrode.

Fig. 3 (a) shows the electrode charge fluctuations on the positive electrode for different compressive stress states. Charging process is found to be composed of two stages: fast charging completed within a few nanoseconds followed by an additional slow charging for maintaining constant electrode charge density. The total simulation time for charging was limited to 2.5 ns as charge fluctuations became minimal and the charging process was completed. At 0 V, the electrolyte is in neutral state. As soon as an externally applied electric field is provided (potential difference), counter ions start moving towards the electrodes almost instantaneously. With increase in potential, the number of counter ions moving towards the electrode increases and thereby forms the double layer almost instantaneously (*Fig. S2*). This represents the fast-charging process observed in *Fig. 3 (a)*. This instantaneous double layer is unstable, therefore, the second part of the charging process, which is much slower as compared to first, the ions rearrange thereby forming a stable double layer. This phenomena of fast charging followed by additional slow charging was also observed by Noh and Jung[32]. With respect to different stress states, the state of zero stress maintains a relatively higher charge density at the end of charging as compared to the stress state 1. This reduction in charge density is found to be proportional to the reduction in mean square displacement (MSD) of the ions due to compression (*Fig. 3 (b)*). MSD provides information as to how easy or difficult it is for the ions to move within the cell during compression or tension. Due to the absence of solvent in EMIM BF_4, compression stress restricts the movement of ions and thus impedes the formation of double layer, which leads to reduction in charge density. The double layer formation has been expanded further in *Section 3.3*. On compressing the EDLC beyond stress state 1, it was found from the MSD plots that there is a detrimental effect on the electrode charge density by 75%. It should be noted that the electrode charge fluctuation and MSD may

not always follow each other with increase in compressive as observed in Fig. 3(b). This could be because even under increasing compressive stress, electrode charge fluctuation is a result of instantaneous double-layer formation while MSD is relatively slower due to slowing down effect of the system.

Fig. 3 (a) compares the electrode charge density at uncompressed (stress state 0), compressed (stress state 1) and stretched conditions (tension). Stretching the EDLC enables charging at a much faster rate as is evident from the steep slope during initial charging phase as compared to zero stress state. This is due to increase in the ionic movement within the cell (*Fig. 3 (b)*) thereby enabling formation of double layer at a much faster rate. An interesting finding from this comparison is that the increase in charge density while stretching the EDLC is merely 7% whereas compressing the EDLC by the same amount reduces the electrode charge density by 29%. Thus, a strong tension-compression asymmetry was observed in the electrode charge density. This asymmetry is well-known to occur in the plastic deformation of metals, especially of BCC type, since dislocation glide prevails in compression while twinning is prominent during tensile pulling of body centred cubic (BCC) metals[33].

This asymmetric electronic behaviour can be explained by considering the distribution of atomic charges on the electrode. *Fig. 4* shows the probability distribution of charges on the

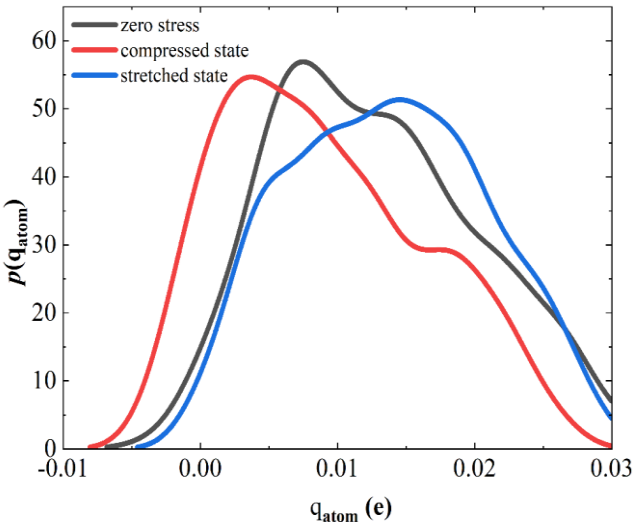

Fig. 4: Probability distribution of electrode charges under zero stress, compressed and stretched states

positive electrode after the charging process is completed (2.5 ns). At positively charged electrode, ideally, a higher atomic charge (q_{atom}) is expected with increase in charge density. For zero stress state, the curve is tilted towards the positive side ($q_{atom} > 0$). For the compressed state, the curve shifts towards left of zero stress state, indicating a reduction in atomic charge on the electrode. This reduction is also observed in *Fig. 3 (b)*. However, the probability of atomic charges in the compressed state reduces by a marginal amount as compared to zero stress state. On the other hand, stretched state provides a higher atomic charge on the electrode, but the probability distribution is lower as compared to the compressed state. An equal probability distribution between compressed and stretched state would provide a similar reduction/increase in charge density on the electrode. With difference in probability distribution of atomic charges, the increment in charge density during stretching (7%) is lower as compared to reduction in charge density during compression (29%).

3.2. Compression at different voltages

The compression effects are further studied at different voltages. Though ionic liquid EDLCs typically operate below 5 V. High-voltage capacitors up to 10 V have also been reported in the literature, where graphene-based electrodes and an ionic liquid electrolyte were used[34]. To

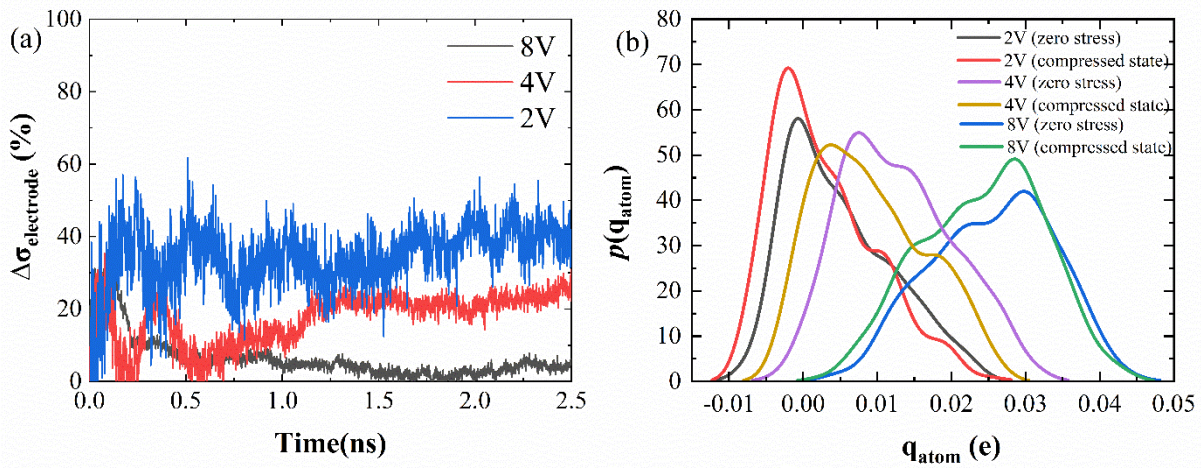

Fig. 5: (a) Percentage change of electrode charge density with respect to zero and compressed states at various potentials (b) probability distribution for positive electrode charge at various potentials. Compressed state refers to stress state 1.

develop a comprehensive understanding of the behaviour of EDLCs over a wide range of voltages, voltages up to 8 V were studied here. The results would also be beneficial for the development of high voltage electrolytes to be used in EDLCs with respect to strain. *Fig. 5 (a)* plots the percentage change in the positive electrode charge density at uncompressed and compressed states for various potentials, which is calculated as

$$\Delta\sigma_{electrode} = \frac{\sigma_{electrode}^{zero} - \sigma_{electrode}^{compressed}}{\sigma_{electrode}^{zero}} \times 100\%. \quad (2)$$

It is found that the percentage variation in electrode charge density reduces with increasing voltages. This indicates that an applied external electric field (due to high potential difference) can tune the electrode charge density regardless of the externally applied stress. As the capacitance of an EDLC is directly related to charge density of electrodes, capacity retention will be better if EDLCs are operated at higher potentials with compression. Another interesting phenomenon observed from *Fig. 5 (a)* are the fluctuations observed in the charge density profiles between the two states at lower potentials and these fluctuations minimise with increase in potential. To explain this phenomenon, the probability distribution of electrode atom charges for zero and compressed states at various potentials are plotted in *Fig. 5 (b)*. Considering the case of $2.0\,V$, the probability distribution profile for compressed state shifts marginally towards left of zero stress state with a higher peak value. This indicates that with compression, charge density tends to shift towards a negative value with high probability, thereby prohibiting the formation of double layer. This leads to high fluctuations between charge density profiles for zero and compressed state states. With increase in potential, the curves shift towards the right indicating rise in charge density (*Fig. S2*). For $4.0\,V$, probability distribution for compressed state shift towards the left of zero stress state; however, the peak value being positive indicates formation of a stable double layer but with reduced charge density as compared to zero stress state (*Fig. S1*). The stable double layer formation leads to

reduced fluctuations in % change between the charge density profiles at $4.0\,V$ as compared to $2.0\,V$ (*Fig. 5 (a)*). With higher potentials of the order of $8.0\,V$, the probability distribution curve shifts farther towards the right and therefore, a higher charge density was obtained (*Fig. S2*). This leads to further increase in the number of charges on the electrode that contributes to forming the double layer, and hence, capacitance will be higher as compared to low potentials for zero as well as compressed stress states. Furthermore, the probability distribution for electrode atom charges for compressed state shifts by a very small amount towards the left of zero stress state, thereby, confirms that charge density on the electrode is retained upon compression as is evident by minimal % changes in charge density for both states (*Fig. 5 (a)*).

3.3. Double layer formation at different stress states

The effect of stress on double layer formation is analysed in detail. The normalised number densities of ions ($EMIM^+$ and BF_4^-) were calculated using OVITO[28] by the following equation

$$n_{ion}^{\pm}(z) = \frac{1}{A}\int_{-x_0}^{x_0}\int_{-y_0}^{y_0} n_{ion}^{\pm}(x', y', z). \tag{3}$$

where $n_{ion}^{\pm}$ is the number density of ions (+ for cations and – for anions). *Fig. 6 (a – c)* compares the normalised number density profiles of ions at different stress states. The profiles of ions from the bulk phase to the first layer of ions near the positive electrode are examined. The oscillating profile of ions is a typical feature of ionic liquid based EDLCs. Normalised density profile of ions reaching a value close to 1 indicates bulk phase which is found for all the cases in *Fig. 6 (a – c)*. This ensures that the central region always forms a bulk phase under all cases of compression.

The first layer of counter ions (BF_4^-) that is closest to the electrode surface is responsible for the formation of double layer. Higher number of counterions and low number of co-ions in the first layer adjacent to the electrode surface can provide a stable double layer with high

capacitance. When there is no compressive stress (i.e., stress state 0), as shown in *Fig. 6 (a)*, the first layer of counter ions with relatively low co-ions provide a stable double layer with equal contribution from the charge storage on the electrode as shown previously in *Fig. 3 (a)*. *Fig. 6 (d)* provides a visual representation and better understanding of the double layer formation in zero stress state. The first layer of counter ion is plotted based on the position of the ions near the electrode surface. A stable layer of counter ions are present at a distance of ≈3.7 Å from the electrode surface. This is followed by an adjacent dispersed layer of co-ions. The dispersion is due to larger size of co-ions ($EMIM^+$) as well as higher MSD for zero stress state allowing the ions to move within the EDLC (*Fig. 3 (b)*).

On comparing the stress state 1 with respect to zero stress state (*Fig. 6 (a & b)*), it can be seen that though the profile of the first layer of co-ions near the electrode surface remains almost similar, the profile of counter ions reduced as compared to zero stress state indicating reduced double layer formation. This reason for this occurrence can be explained based on the

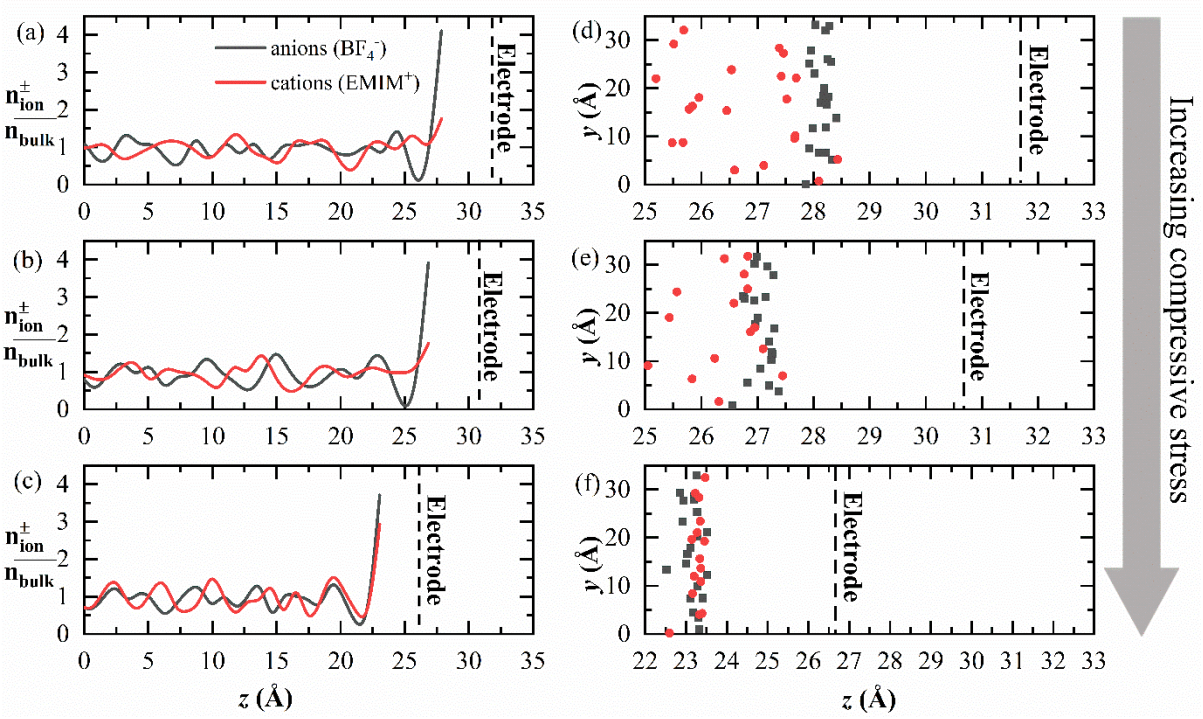

Fig. 6: Variation of normalised number density profile of ions near the positive electrode (a, b, c) and corresponding double layer formation (d, e, f) with respect to zero stress, stress state 1 and stress state 5 respectively. Black squares represent the counter ions (anion, BF_4^-) and red circle indicates the co-ions (cation, $EMIM^+$). The dotted lines represent the position of positive electrode.

position of ions forming the double layer in *Fig. 6 (d & e)*. As the EDLC is compressed, the position of electrode shifts inwards, this also shifts the counter ions forming the double layer by equal amounts (distance between 1st layer of counter ions and electrode surface remains similar i.e. ≈3.7 Å). However, with compression, the MSD of the ionic liquid reduces (*Fig. 3 (b)*), as a result of which the co-ions that were originally in dispersed state adjacent to the 1st layer of counter ions, fail to displace uniformly as compared to the 1st layer of counter ions. Due to this, some of the co-ions overlap with the counter ions thereby reducing the amount of counter ions available for the double layer formation with the electrode surface. This leads to reduction in double layer formation and thereby reduces the amount of charge storage in the electrode surface (*Fig. 3 (a)*).

With increased compression, the counter ions in the 1st layer reduces and the co-ions increases (*Fig. 6 (c)*). Therefore, the available number of counter ions responsible for double layer formation decreases drastically, leading to substantial decrease in the amount of charge storage in the electrode at higher rates of compression. The process of electrode movement shifting the counter ions by equal distance remains valid even for higher states of compression. With very low MSD at high rates of compression (*Fig. 3 (b)*), the movement of co-ions reduces further and this leads to overlapping of a large number of co-ions with the counter ions at stress state 5 as compared to zero stress state and stress state 1 (*Fig. 6 (f)*).

Fig. 7 (a) shows the case where the EDLC is stretched. Under such conditions, the double layer formation is more stable as compared to zero stress state. This can be confirmed by the relative positions of counter ions with respect to electrode surface. During stretching majority of counter ions are available near to the electrode surface which facilitates double layer formation whereas in the case of zero stress state, though there are sufficient number of counter ions available, however, near to the electrode surface, only a partial number of counter ions participate in contributing to double layer formation. This can be further verified by the

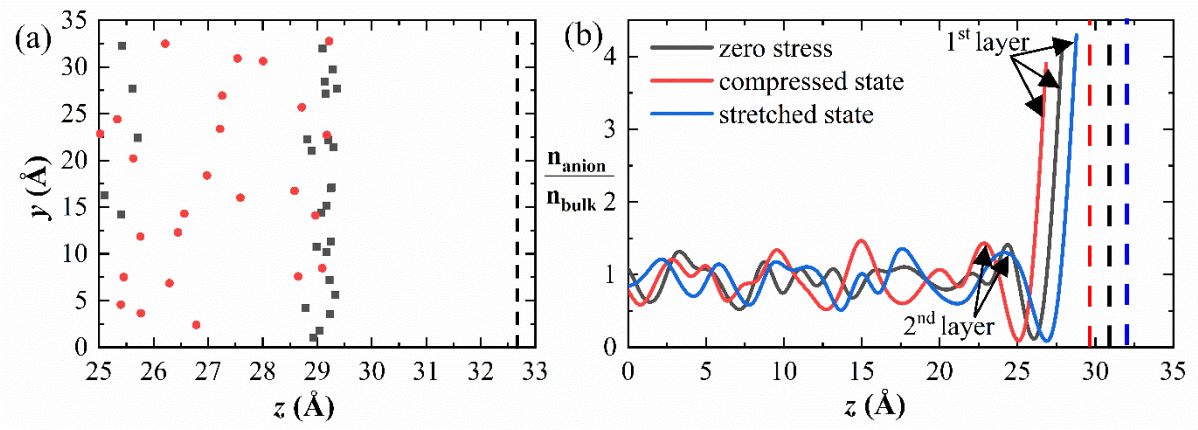

Fig. 7: (a) Double layer formation with respect to tensile strain (b) Comparative analysis of non-dimensional number density profile of counter ions (anions) near the positive electrode during stretching and compression of EDLC. Compressed state indicates stress state 1. Black squares represent the counter ions (anion, BF_4^-) and red circle indicates the co-ions (cation, $EMIM^+$). The dotted lines represent the positive electrode

normalised number density profiles of anions where stretched state has a higher profile of counter ions as compared to zero stress state (*Fig. 7 (b)*). Also, due to higher MSD for ionic liquid at stretched state (*Fig. 3 (b)*), the 1st and 2nd layer of counter ions are formed with sufficient spacing to allow for a layer of co-ions to form between them as compared to other two states compared in *Fig. 7 (b)*. Another validation for this claim is that the 7% increase in electrode charge density at stretched state as compared to zero stress state as already discussed previously based on *Figs. 4 (a & c)*.

Areal capacitance provides a measure of the ability of the EDLC to store charge at a fixed potential difference between the electrodes. The areal capacitance for all the cases simulated in this study (under compression and tension) is plotted in *Fig. 8* and calculated by

$$C_{DL} = \frac{\sigma_{electrode}}{\varphi}. \tag{4}$$

where C_{DL} indicates the areal capacitance with respect to the positive electrode ($\mu F/cm^2$) and φ indicates applied potential (V). Compressing the EDLC from zero stress (2.09 µF/cm^2) to stress state 1 reduces the capacitance by a significant amount. Any further compression beyond stress state 1, a very low amount of capacitance is obtained of about 0.5 µF/cm^2. On the other hand, stretching the EDLC results in a higher value of capacitance. The reason for this being a

large number of counter ions forming the double layer due to enhanced MSD of ions leading to subsequent increase in charge storage in the electrode. It should also be noted that there is a negligible increase in the areal capacitance beyond stress state 4 (for stress state 5 which is similar to stress state 3), as observed in *Fig. 8*, which could be due to the involvement of a few new counter ions in double-layer formation. From Fig. 6 (a – c), it could be observed that there are few numbers of counter ions distributed away from the positive electrodes and initially are not contributing towards the double-layer formation. It can also be noted that the distribution of these counter ions is also varying with respect to the compressive stress. Hence, at stress state 5, these counter ions (which were not initially contributing towards the double-layer formation) came close to the positive electrode and contributed towards areal capacitance. *Fig. 9* shows the schematic of the electrochemical behaviour of the EDLC under stretched, zero stress, compressed state and from the schematic it could be clearly observed that the counter ions contributing towards capacitance is varying under compressed, stretched and zero stress conditions.

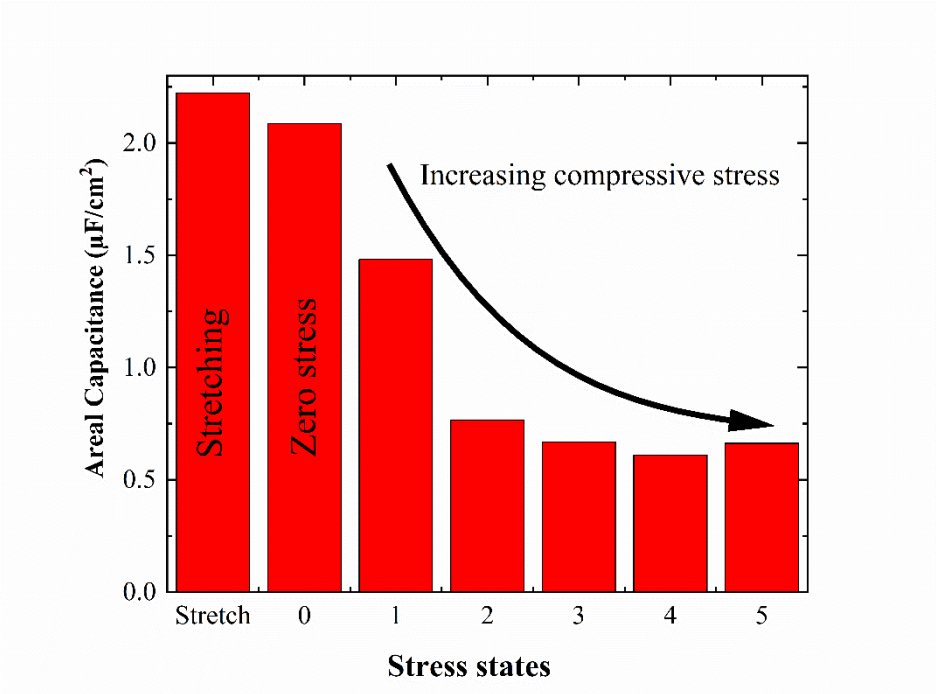

Fig. 8: Areal capacitance of the EDLC at 4V with respect to compression and tension of EDLC

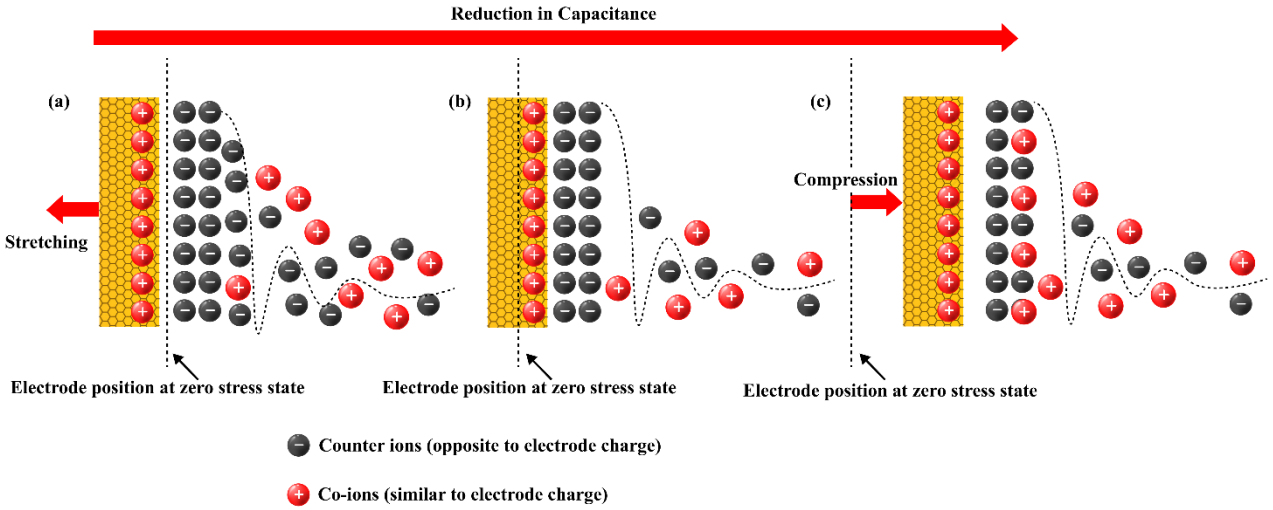

Fig. 9: Schematic explaining the electrochemical behavior of the EDLC under (a) Stretched state, (b) Zero stress state, (c) Compression

3.4. Relevance of MD results with previously reported experimental results

Experimental evidences show limited increase in the capacitance with increasing compressive stresses[13] as well as a substantial deterioration in the performance has also been reported. The deterioration has been attributed to the alteration of physical structure of electrode upon compression and electrolyte displacement. Our findings show the deterioration in performance of EDLCs during compression due to the displacement of ionic liquid (electrolyte). Reported experiments in the past have made use of a nanoporous electrode, which is responsible for the initial increase in the capacitance, however, the system simulated in this work considers an atomically flat 2D crystalline electrode of a defect free graphene. If nano porous electrodes are designed for EDLCs, the coupled effect of physical alteration of electrode structure along with ionic liquid displacement leading to reduced performance of EDLCs can be studied.

With regards to stretching, elastic and deformable material for electrodes are considered in experiments which can accommodate high degree of tensile strain[17,18]. With current limitations in modelling the stretchable geometries for electrode materials, a simple case of

stretching was considered in this study that showed an enhancement in the performance of EDLC. Advanced models with realistic geometries can elucidate a better insight of the physics of double layer formation at the fundamental level can be explored. Perhaps a more important point to note here is that the strain rate typically used in the displacement controlled tensile tests in the MD simulation are substantially higher than experiments and this limitation applies even to the publications reported on nanoscale tensile tests of nanowire[35,36]. The sensitivity of the applied strain-rate can make a difference on the reported electrochemical performance of the ionic liquid, and this would be an interesting follow on study to be looked at. With advancement in modelling deformable geometries upon tension, a better understanding of the physics of double layer formation at the fundamental level can be explored.

4. Conclusions

In this work, the electrochemical behaviour of an ionic liquid based Electrochemical Double Layer Capacitor (EDLC) under the influence of applied external stresses and voltages were modelled using molecular dynamics by placing an EMIM BF_4 electrolyte between two graphene electrodes. Analogous to the tension-compression asymmetry observed during mechanical deformation of solid BCC metals, a similar tension-compression asymmetry herein was observed in the electrode charge density of an EDLC. For instance, low compression of EDLC showed a reduced performance in terms of charge density in the electrodes (29%). This reduction substantially deteriorated with increased compression. Stretching or tensile strain, on the other hand, enhance the performance by increasing the charge storage capacity of the electrode by 7%. The reduction and enhancement in performance of an EDLC respectively with compression and stretching was attributed to two reasons: (a) electrode movement leads to shifting the first layer of counter ions by equal amounts and (b) mean square displacement of ions prohibiting/allowing the movement of co-ions during compression/stretching, thereby

limiting/allowing the number of counter ions available for double layer formation. The higher the potential, the better the capacity retention with compression is. Practical EDLCs involves porous electrodes and an applied strain, can alter the porous structure, thereby affecting the performance. However, the present study considered theoretically flat electrodes. Further understanding can be achieved in future by designing porous electrodes of different pore sizes to study the performance of EDLCs with ionic liquids under different rates of compression and tension at different strain rates.

Author contributions

TR – Conceptualization, Data curation, Formal Analysis, Investigation, Methodology, Software, Validation, Visualization, Writing – original draft, Writing – review & editing

SG – Data curation, Formal Analysis, Investigation, Methodology, Software, Supervision, Validation, Visualization, Writing – review & editing

LC – Data curation, Formal Analysis, Supervision, Visualization, Writing – review & editing

MM – Investigation, Supervision, Validation, Visualization, Writing – review & editing

GO –Funding acquisition, Investigation, Project administration, Resources, Software, Supervision, Validation, Visualization, Writing – review & editing

MM –Funding acquisition, Investigation, Project administration, Resources, Software, Supervision, Validation, Visualization, Writing – review & editing

HW – Conceptualization, Funding acquisition, Investigation, Methodology, Project administration, Resources, Software, Supervision, Validation, Visualization, Writing – review & editing

Conflicts of interest

There are no conflicts to declare

Research data Statement

All data can be accessed from https://doi.org/10.5281/zenodo.4065552

Acknowledgements

TR, GO, MM, HW acknowledges the financial support provided by the Innovate UK WIZer project (TS/S005811/1). TR acknowledges the financial support provided by the Science and Engineering Research Board (SERB), Government of India (SRG/2021/000741). SG would like to acknowledge the financial support provided by the UKRI via Grants No. EP/S036180/1 and EP/T024607/1, Hubert Curien Partnership Programme from the British Counsil and the International exchange Cost Share award by the Royal Society (IEC\NSFC\223536). HW greatly acknowledges the financial support provided by the UKRI via Grant No. EP/S000933/1. LTC thanks the PRINT-UFF/CAPES project, 7.310459/2018-00 and CNPq for the fellowship. The work used Imperial College Research Computing Service, DOI: 10.14469/hpc/2232. Additionally, we are gratefully thankful for receiving access to various HPC resources including the Isambard Bristol, UK as well as Kittrick (LSBU), Magus 2 at Shiv Nadar University and Param Ishan (IIT Guwahati, India).

References

1. F. Constanze, *ESDN Report*, **53**, (2020).
2. C. E. Sandy Thomas, *Int. J. Hydrogen Energy*, **34**, 9279–9296 (2009).
3. W. Sarwar et al., *J. Power Sources* (2016).
4. L. H. Saw et al., *Energy Procedia*, **158**, 2750–2755 (2019).
5. S. Yu, D. Lin, Z. Sun, and D. He, *Int. J. Energy Res.*, **44**, 7495–7506 (2020).
6. D. A. C. Brownson, D. K. Kampouris, and C. E. Banks, *J. Power Sources*, **196**, 4873–4885 (2011).
7. X. Huang, Z. Zeng, Z. Fan, J. Liu, and H. Zhang, *Adv. Mater.*, **24**, 5979–6004 (2012).
8. L. Yu and G. Z. Chen, *Front. Chem.*, **7**, 1–15 (2019).
9. M. Galiński, A. Lewandowski, and I. Stepniak, *Electrochim. Acta*, **51**, 5567–5580 (2006).

10. H. Park et al., *Nano Energy*, **83**, 105837 (2021) https://doi.org/10.1016/j.nanoen.2021.105837.

11. X. Li, J. Rong, and B. Wei, *ACS Nano*, **4**, 6039–6049 (2010).

12. M. Hu et al., *Chem. Commun.*, **54**, 6200–6203 (2018).

13. G. Gourdin, A. Meehan, T. Jiang, P. Smith, and D. Qu, *J. Power Sources*, **196**, 523–529 (2011).

14. G. Gourdin, T. Jiang, P. Smith, and D. Qu, *J. Power Sources*, **215**, 179–187 (2012).

15. P. Lv et al., *Nanoscale Res. Lett.*, **12** (2017).

16. P. Li et al., *Nanoscale*, **5**, 8472–8479 (2013).

17. I. K. Moon, B. Ki, and J. Oh, *Chem. Eng. J.*, **392**, 123794 (2020).

18. C. R. Chen, H. Qin, H. P. Cong, and S. H. Yu, *Adv. Mater.*, **31**, 1–10 (2019).

19. Q. Liang et al., *Chem. Eng. J.*, **427**, 131904 (2022) https://doi.org/10.1016/j.cej.2021.131904.

20. N. Bai et al., *Electrochim. Acta*, **249**, 360–368 (2017) http://dx.doi.org/10.1016/j.electacta.2017.08.034.

21. Y. Ko et al., *Nat. Commun.*, **2017**, 1–10 http://dx.doi.org/10.1038/s41467-017-00550-3.

22. Q. Xin et al; *Acs Appl. Electron. Mater*, **5**, 3756-3764, (2023)

https://doi.org/10.1021/acsaelm.3c00476

23. M. Kroupa, G. J. Offer, and J. Kosek, *J. Electrochem. Soc.*, **163**, A2475 (2016).

24. M. Z. Bazant, B. D. Storey, and A. A. Kornyshev, *Phys. Rev. Lett.* (2011).

25. S. Kazemiabnavi, Z. Zhang, K. Thornton, and S. Banerjee, *J. Phys. Chem. B*, **120**, 5691–5702 (2016).

26. L. Martinez, R. Andrade, E. G. Birgin, and J. M. Martínez, *J. Comput. Chem.* (2009).

27. S. Plimpton, *J. Comput. Phys.*, **117**, 1–19 (1995).

28. A. Stukowski, *Model. Simul. Mater. Sci. Eng.*, **18** (2010).

29. J. N. Canongia Lopes, J. Deschamps, and A. A. H. Pádua, *J. Phys. Chem. B*, **108**, 2038–2047 (2004).

30. S. Goel et al., *Mater. Today Chem.*, **18**, 100356 (2020).

31. Z. Wang, Y. Yang, D. L. Olmsted, M. Asta, and B. B. Laird, *J. Chem. Phys.*, **141**, 1–6 (2014).

32. C. Noh and Y. Jung, *Phys. Chem. Chem. Phys.*, **21**, 6790–6800 (2019).

33. S. Goel, B. Beake, C. W. Chan, N. Haque Faisal, and N. Dunne, *Mater. Sci. Eng. A*, **627**, 249–261 (2015).

34. T. Romann, O. Oll, P. Pikma, K. Kirsimäe, and E. Lust, *J. Power Sources*, **280**, 606–611 (2015).

35. S. Goel, A. Kovalchenko, A. Stukowski, and G. Cross, *Acta Mater.*, **105**, 464–478 (2016).

36. S. Goel et al., *Comput. Mater. Sci.*, **152**, 196–210 (2018).